Journal of Power Sources 191 (2009) 400–406

Contents lists available at ScienceDirect

Journal of Power Sources

journal homepage: www.elsevier.com/locate/jpowsour

The effect of internal air bleed on CO poisoning in a proton exchange membrane fuel cell

Wentao Wang*

Department of Chemical Engineering, University of South Carolina, Columbia, SC 29208, United States

ARTICLE INFO

Article history:
Received 30 December 2008
Received in revised form 18 February 2009
Accepted 19 February 2009
Available online 4 March 2009

Keywords:
Proton exchange membrane
CO poisoning
Fuel cells
Air bleed
Catalyst-coated membrane

ABSTRACT

It is found that carbon monoxide (CO) poisoning could be mitigated by increasing only cathode back-pressure for a proton exchange membrane fuel cell (PEMFC) with ultra-thin membranes (≤25 μm). This mitigation can be explained by a heterogeneous oxidation of CO on a Pt–Ru/C anode by the permeated O_2 which is known as "internal air bleed" in his paper. A steady-state model which accounts for this internal air bleed has been developed to model the Pt–Ru/C anode polarization data when 50 ppm CO in H_2 is used as anode feed gas. The modeling results show that the mitigation of CO poisoning by the internal air bleed even exists at ambient conditions for a PEMFC with an ultra-thin membrane. Therefore, the effect of internal air bleed must be considered for modeling fuel cell performance or anode polarization data if an ultra-thin membrane and a low level of CO concentration are used for a Pt–Ru/C anode. An empirical relationship between the amount of internal air bleed used for the mitigation of CO poisoning and the fraction of free Pt sites is provided to facilitate the inclusion of an internal air bleed term in the modeling of anode polarization and the fuel cell performance.

1. Introduction

The proton exchange membrane fuel cell (PEMFC) is promising for transportation and stationary applications power due to high fuel efficiency, quick start-up, and high power density under low temperatures. However, carbon monoxide (CO) poisoning has been a major barrier to the commercialization of PEMFCs. It has been demonstrated very early that even a small amount of CO as low as 10 ppm in anode feed stream could cause considerable performance loss when Pt/C was used as anode catalyst [1].

Extensive research has been devoted to the mitigation of CO poisoning in a PEMFC. Gottesfeld and Pafford [2] first presented the oxygen bleeding technique to reduce CO poisoning by mixing 2–5 vol% O_2 with anode fuel containing 100 ppm CO. The mitigation mechanism of oxygen bleeding technique is the heterogeneous oxidation of CO by O_2 to CO_2 [3]. CO poisoning can also be mitigated by using dilute (5 vol%) and oxygen-evolving H_2O_2 in an anode humidifier for a 100 ppm CO in a H_2 feed [4], which was reduced to less than 1 vol% by Bellows et al. [5] to mitigate the same CO level in the anode feed. The mitigation mechanism for dilute H_2O_2 was found to be the slow decomposition of H_2O_2 to O_2 in the stainless steel anode humidifier instead of H_2O_2 vapor decomposition on a catalyst.

Another approach to alleviating CO poisoning is use CO-tolerant Pt-alloys as anode catalysts, such as Pt–Ru [6–12], Pt–Sn [6,7], Pt–Ti [13], and Pt–Mo [14–17], or Pt–Ru–Mo [18]. Pt–Ru is the most commonly used anode catalyst among all the CO-tolerant Pt–M catalysts. The mechanism of better CO-tolerance for Pt–Ru is either due to the fact that H_2O adsorbs on the alloying Ru at lower potential compared with Pt [19–21] or CO adsorbs on Pt less strongly due to the presence of the alloying Ru [22]. The effect of oxygen bleed or air bleed can be enhanced when combining a CO-tolerant anode. Murthy et al. [23] reported that single cell performance could be restored for a PEMFC operating with 500 ppm CO in an anode feed when a CO-tolerant Pt-alloy and a 5 vol% air bleed were used for the anode. Performance could be recovered a lot for 3000 ppm CO when a higher air bleed (15 vol%) was used. For a 5 vol% air bleed, a higher CO-tolerance (~1000 ppm CO/H_2) could be achieved for a Pt–Ru anode if a Ni-foam sheet filled with Fe_2O_3–Au powder was placed before the anode [24]. The purpose of using Fe_2O_3 is because the rate of selective oxidation of CO by O_2 on Au/Fe interface is high at normal fuel cell operational conditions. Shi et al. [25] reported recently a novel anode with Pt- or Au-refined diffusion layer, which enhances considerably the efficiency of a 2% air bleed.

Haug et al. proposed a less expensive Ru filter consisting of carbon-supported Ru and Nafion® solids [26] or sputter-deposited Ru layer(s) separated by Nafion-carbon ink [27]. This Ru filter could be placed on top of a Pt anode to increase the CO tolerance with a low-level air bleed. According to their work, the increased CO tolerance of Ru filter is primarily because of the formation of Ru–OH from the O_2 in the air bleed. Furthermore, the kinetics of H_2 adsorp-

* Present address: E2TAC, College of Nanoscale Science and Engineering, University at Albany, State University of New York, Albany, NY 12203, United States. Tel.: +1 803 777 4181; fax: +1 803 777 8265.
E-mail address: wentao_sc@hotmail.com.

0378-7753/$ – see front matter © 2009 Elsevier B.V. All rights reserved.
doi:10.1016/j.jpowsour.2009.02.058

Nomenclature

b_{fc}	back-to-forward CO adsorption ratio (Pa)
b_{fh}	back-to-forward H_2 adsorption ratio (Pa)
c_{O_2}	concentration of O_2 in the CCM (mol cm^{-3})
$c^0_{O_2}$	pre-exponential factor (mol cm^{-3})
c_t	molar area density of catalyst site (mol cm^{-2})
D_{O_2}	diffusion coefficient of O_2 (cm^2 s^{-1})
$D^0_{O_2}$	pre-exponential factor (cm^2 s^{-1})
E_{diff}	activation energy for diffusion (J mol^{-1})
F	Faraday's constant (96,485 C mol^{-1})
ΔG_{diss}	free energy of dissolution (J mol^{-1})
i	current density of fuel cell (A cm^{-2})
i_h	current density from hydrogen oxidation (A cm^{-2})
k_1	rate constant for O_2 dissociation on Pt (mol cm^{-2} s^{-1} Pa^{-1})
k_{CO}	rate constant for oxidation of Pt–CO by Pt–O (mol cm^{-2} s^{-1})
k_{eh}	hydrogen electro-oxidation rate constant (mol cm^{-2} s^{-1})
k_{fc}	electrode forward CO adsorption rate constant (mol cm^{-2} s^{-1} Pa^{-1})
k_{fh}	electrode forward H_2 adsorption rate constant (mol cm^{-2} s^{-1} Pa^{-1})
n	number of electrons involved in H_2 oxidation, which is equal to 2
N_{O_2}	flux of O_2 through membrane (mol cm^{-2} s^{-1})
K_{eq}	equilibrium constant (Pa$^{-1/2}$)
K_H	Henry's constant for air-equilibrated membrane (kPa cm^3 mol^{-1})
p_{atm}	atmospheric pressure (101.325 kPa)
p_{CO}	partial pressure of CO in the humidified gas (Pa)
p_{O_2}	partial pressure of O_2 in the humidified gas (Pa)
p_{sat}	saturated water vapor pressure (Pa)
P_t	total cathode backpressure (Pa)
r	reaction rate (mol cm^{-2} s^{-1})
R	universal constant (8.314 J mol^{-1} K^{-1})
t	time (s)
t_m	membrane thickness (cm)
T	absolute temperature (K)
V_{H_2}	cell voltage for (H_2, air) system at a given current density (V)
V_{CO/H_2}	cell voltage for (CO/H_2, air) system at a given current density (V)

Greek letters

β_{H_2}	transfer coefficient of H_2
γ	fraction of permeated O_2 used for oxidation of CO
η_a	anode overpotential (V)
$\eta_{a,ex}$	experimental anode overpotential (V)
$\eta_{a,th}$	predicted anode overpotential (V)
θ_{CO}, θ_{H_2}	fractional coverage of CO, H_2
θ_M	fraction of free Pt sites

tion on Ru is a few orders of magnitude slower than that on Pt, the lower concentration of H_2 on the Ru filter increases the probability of reaction between Ru–OH and Ru–CO. A reconfigured anode containing inexpensive transition metal oxides (*e.g.*, CuO and Fe_2O_3) coating on the gas diffusion layer could also be employed to oxidize CO with a 6-vol% air bleed before the anode feed reaches the anode active layer [28]. A tolerance to 100 ppm CO in H_2 is achievable for this reconfigured anode when using a Pt anode with low catalyst loading. Adcock et al. [29] further demonstrated that the CO tolerance of a Pt anode could be raised to the same level as that of a CO-tolerant Pt–Ru anode with similar Pt loading if a reconfigured anode and a small amount of air bleed were used.

The rates of hydrogen and oxygen crossover may influence the fuel cell reactions occurring on anode and cathode sides and subsequently the cell performance of the whole fuel cell. The diffusion properties of H_2 and O_2 through the Nafion® membranes have been examined extensively and some of these papers used a Nafion® membrane with a pressed-on catalyst [30–34]. Others used a cylindrical microelectrode with pressed-on Nafion® membrane [35–37]. Regardless of the electrodes used, they employed the same technique by setting the electrode potential high or low enough so that H_2 or O_2 was oxidized or reduced under mass transfer limited conditions. Diffusion coefficients or solubility could be determined by using all or part of the data points. Relatively thick membranes were used for the studies of permeability of membranes.

Zhang et al. examined the effect of oxygen permeation on the PEMFC performance with Nafion® 115 (125 μm) and 117 (175 μm) as a function of anode flow rates corresponding to stoichiometries much greater than 1.2 and estimated a selectivity coefficient for the reaction of diffused O_2 with the adsorbed CO on a Pt/C anode with a CO inventory model [38]. It was further shown by Zhang et al. that no significant mitigation of CO poisoning effect by diffused O_2 could be observed for Nafion® 115 (125 μm) if air was used as cathode feed gas. However, the crossover rate of O_2 from cathode to anode could be much larger for catalyst-coated membranes (CCMs) fabricated with ultra-thin (≤25 μm) membranes when air is used for cathode. The work presented here is to examine the effect of diffused O_2, which is known as internal air bleed in this paper, on the mitigation of CO poisoning for a CO-tolerant Pt–Ru/C anode with ultra-thin membranes. A model which accounts for the diffusion of the dissolved O_2 through the membrane, the adsorption of O_2 in the anode catalyst, and the subsequent surface reaction of O_2 with CO will be used to predict the anode overpotential.

2. Experimental

The fuel cell used in the experiment was a 25-cm^2 single cell with a triple serpentine flow field manufactured by Fuel Cell Technology, Inc. Multiple CCMs were used in the experiments. They were reproducible to within ±5 mV at a given current and they consisted of a 0.45 mg cm^{-2} Pt–Ru (1:1) on carbon anode and a 0.4 mg cm^{-2} Pt on carbon cathode deposited onto either a 5 or 25 μm Gore Select® membrane. The Pt–Ru(1:1) catalyst for anode is supported on Vulcan XG-72. The weight percentages of Pt and Ru are 33% and 17%, respectively. The Pt catalyst for cathode is supported on Vulcan XC-72 and the weight percentage of Pt is 50%. Both catalysts are from Tanaka Kikinzoku Group. The weight ratio of carbon to Nafion ionomer is 0.35:0.5 in both anode and cathode catalyst layers. The thickness of the anode or the cathode coating was about 12.5 μm. CARBEL™ CL Gas Diffusion Media (0.4 mm) from W.L. Gore & Associates, Inc. was used and compressible gaskets (0.25 mm) were inserted between flow field plates and the CCM to prevent fuel gases from leaking. The active area of the fuel cell was 20 cm^2 because two sub-gaskets (25 μm) with a 20-cm^2 window were inserted between the CCM and the compressible gaskets.

The gas flow rates, humidification bottle temperature were controlled with a test station (Model 891) made by Scribner Associates, Inc. The fuel gas for the anode was either ultra-high purity hydrogen or CO/H_2 and the gas for cathode was industrial grade air. The cell temperature was 70 °C. The gases of anode and cathode were humidified by passing the gas through deionized (DI) water and the correlation of dew points and humidification temperatures were measured as described in Ref. [39]. For the 25 μm CCM, the humidification temperatures were 85 and 75 °C, respectively. The

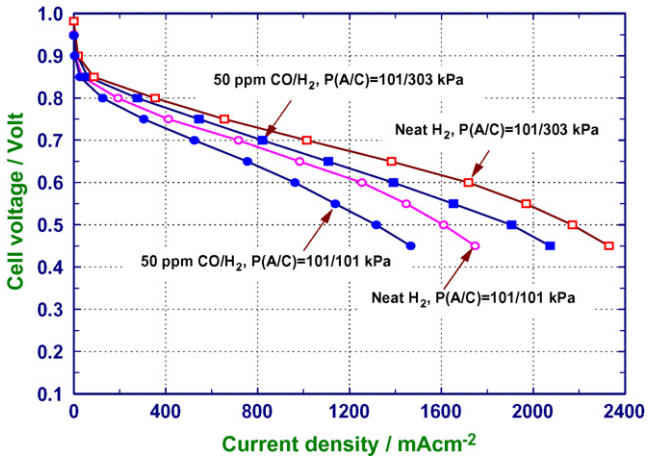

Fig. 1. The effect of cathode backpressure on PEMFC performance for 25 μm CCM with 50 ppm CO/H_2 and data shown for neat H_2. T_{cell} = 70 °C, T_D(A/C) = 80/70 °C. Closed symbols are for CO/H_2, and open symbols are for H_2. 101 kPa (● and ○) 303 kPa (■ and □).

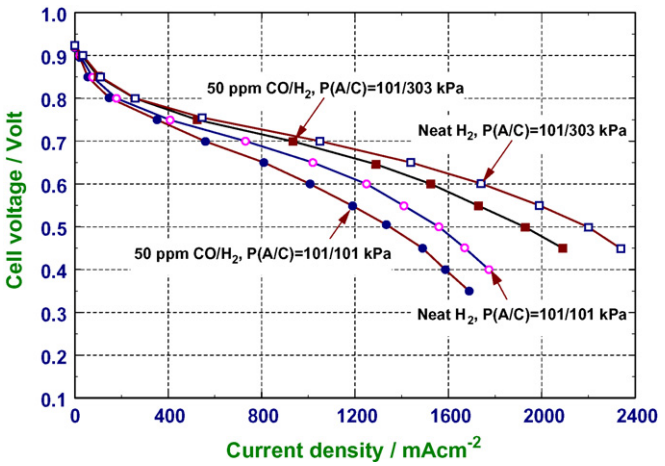

Fig. 2. The effect of cathode backpressure on PEMFC performance for 5 μm CCM with 50 ppm CO/H_2 and data shown for neat H_2. T_{cell} = 70 °C, T_D(A/C) = 70/60 °C. Closed symbols are for CO/H_2, and open symbols are for H_2. 101 kPa (● and ○) 303 kPa (■ and □).

humidification temperatures for the 5 μm CCM were 75 and 65 °C for anode and cathode, respectively, corresponding to dew points of 70 and 60 °C. The reason why relatively lower humidification temperatures were used for 5 μm CCM is because it is thinner and less water is needed to make it well hydrated. The stoichiometry for the normal fuel cell operation was 1.2 for anode (dry H_2 base) and 2.0 for cathode. In this work, each new CCM was subjected to a constant-voltage three-step 70-h incubation procedure before the new CCM was used in the experiments.

In the experiments, the steady-state current–voltage polarization curves were obtained in neat H_2 and in a mixture of 50 ppm CO/H_2. Two different sets of backpressures, P(A/C) = 101/101 kPa and P(A/C) = 101/303 kPa, were used for anode and cathode. Note that only the cathode backpressure was changed in an effort to maintain a constant dynamic hydrogen reference electrode. For each CCM, current–voltage curves were obtained with neat H_2 under different backpressures before it was exposed to CO/H_2 so that a baseline could be established. For the polarization curve, the cell voltages were arranged in a random sequence to remove hysteresis and ensure reproducible data. After the cell voltage was set, the test station changed the flow rates automatically based on the current to obtain the desired stoics of 1.2 and 2.0. Note that the mass flow controllers used in the experiments had a minimum flow rate of 50 standard $cm^3\ min^{-1}$ (sccm)[1]. Thus the gas flow rate would be kept at 50 sccm if the flow rate is smaller than 50 sccm based on stoics. Multiple CCMs were used during the experiments. The polarization curves for the same type of CCMs were within ±5% of the current at the same cell voltage. For a given CCM, there was no difference in the polarization curves with neat H_2 before and after the experiments.

3. Results and discussion

3.1. Effects of cathode backpressure and membrane thickness on cell performance

Figs. 1 and 2 show the steady-state current–voltage curves for neat H_2 and 50 ppm CO/H_2 mixture for 25 and 5 μm CCMs under different cathode backpressures. The cell performance increases as the backpressure of air increases for both neat H_2 and 50 ppm CO/H_2 mixture, as shown in Figs. 1 and 2. Figs. 3 and 4 present anode

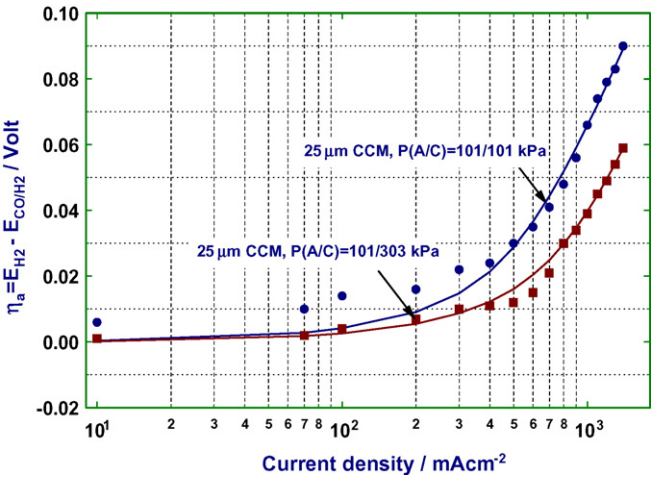

Fig. 3. Comparison of anode overpotential between the model prediction and experimental data for 25 μm CCM with 50 ppm CO/H_2. T_{cell} = 70 °C, T_D(A/C) = 80/70 °C, Stoic.(A/C) = 1.2/2.0. (●) Whole-cell anode polarization when P(A/C) = 101/101 kPa, (■) whole-cell anode polarization when P(A/C) = 101/303 kPa, (—) model prediction.

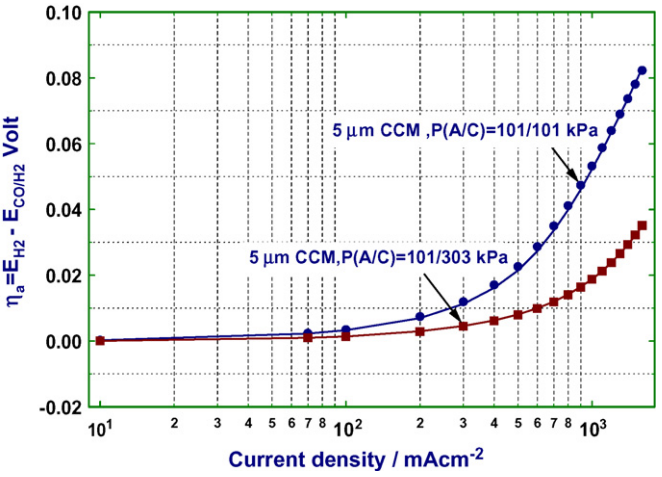

Fig. 4. Comparison of anode overpotential between the model prediction and experimental data for 5 μm CCM with 50 ppm CO/H_2. T_{cell} = 70 °C, T_D(A/C) = 70/60 °C, Stoic.(A/C) = 1.2/2.0. (●) Whole-cell anode polarization when P(A/C) = 101/101 kPa, (■) whole-cell anode polarization when P(A/C) = 101/303 kPa, (—) model prediction.

[1] Our standard conditions refer to 273 K and 101 kPa.

overpotential data obtained by subtracting the cell potential with CO/H_2 from the cell potential with neat hydrogen at the same current density. Therefore, to call this overpotential, it is assumed that the hydrogen overpotential with neat hydrogen is negligible, that CO does not affect the thermodynamic voltage of either electrode, and that the ohmic contribution to the cell voltage and the cathodic overpotential depend only on the current density. Since the oxidation of H_2 on Pt or Pt/Ru is very fast, η_{H_2} is small and negligible, the anode polarization due to the presence of CO in the anode gas stream can be written as the difference between the cell voltages under the same current density.

$$\eta_a \approx V_{H_2} - V_{CO/H_2} \quad (1)$$

These overpotential data allows us to compare the effect of internal air bleed on CO poisoning when the baseline performances are different. If there is no oxygen crossover in the PEM fuel cell, the anode polarization under different cathode backpressures should be the same. However, it is indicated very clearly in Figs. 3 and 4 that the anode polarization decreases with the increase of cathode backpressure or a thinner CCM is used.

Du et al. [40] demonstrated that there was a decrease in CO concentration when reformate gas containing 10.53 ppm CO was passed through anode at open circuit condition. It is obvious that oxygen crossover plays an important role in the partial removal of CO for the ultra-thin CCMs under high cathode backpressure. However, the internal air bleed cannot remove all adsorbed CO on the anode catalyst surface because the performance of 50 ppm CO/H_2 is still lower than that of neat H_2 even when the cathode backpressure is increased to 303 kPa. The diffusion coefficient of O_2 through membrane is larger and CO sticking coefficient on Pt is less under higher cell temperatures, so it is expected that this internal air bleeding technique may be more effective under relatively higher cell temperatures (>70 °C).

3.2. Calculation of O_2 crossover through membranes

The flux of O_2 through membrane is a critical parameter for modeling of the effect of internal air bleed on CO poisoning. Gore Select® membrane is a composite membrane reinforced with a microporous, expanded polytetrafluoroethylene (e-PTFE). It is manufactured by impregnating the porous e-PTFE with Nafion® resin. The porosity of the porous e-PTFE could be as high as 95% and almost all the interior volume of the e-PTFE is filled by Nafion® resin [41]. This means Gore Select® membrane is composed primarily of Nafion® resin. The 5 and 25 μm Gore Select® membranes look transparent, very much like the non-reinforced Nafion® membrane. Both kinds of Gore Select® membranes appear to be uniform and homogeneous. According to Liu et al. [42], the hydrogen crossover rate of a 25 μm Gore Select® membrane is similar to that of a 25 μm Nafion® 101. For these reasons, 5 and 25 μm Gore Select® membranes can be treated as Nafion® membranes with the same thicknesses in estimating oxygen diffusion coefficient and oxygen crossover rate without introducing too much error. Under mass transfer limited condition, the flux of O_2 through Gore Select® membrane can be written as follows:

$$N_{O_2} = \frac{D_{O_2} c_{O_2}}{t_m} \quad (2)$$

where D_{O_2} is the diffusion coefficient of O_2 in the membrane and c_{O_2} is the solubility of O_2 in the membrane. Diffusion coefficient and solubility of O_2 in membranes are routinely measured by the electrochemical monitoring technique developed by Devanathan and Stachurski [43]. Ogumi et al. investigated the permeation of O_2 through Nafion® 120 and Nafion® 117 of different ionic types in sulfate salt media using the electrochemical monitoring technique and determined the diffusion coefficient and solubility of O_2 using only part of the data [30,31]. Kimble et al. presented a more accurate nonlinear parameter estimation technique to determine the diffusion coefficient and solubility of gases by using all the experimental data [44]. Haug and White estimated the diffusion coefficient and solubility of O_2 through the H^+ Nafion® 117 and Cape Cod membranes in 0.5 M H_2SO_4 medium employing the above-mentioned nonlinear parameter estimation technique [34]. Parthasarathy et al. did thorough research on temperature and pressure dependence of O_2 diffusion coefficient and solubility in H^+ Nafion® membrane under conditions which are similar to an operating PEM fuel cell [45,46]. According to Parthasarathy et al., the diffusion coefficient of O_2 in hydrated H^+ Nafion® membrane is independent of partial pressure of O_2. However, its dependence on temperature follows an Arrhenius relationship:

$$D_{O_2} = D^0_{O_2} \exp\left(-\frac{E_{diff}}{RT}\right) \quad (3)$$

A similar equation can be used to describe the dependence of solubility of O_2 on temperature:

$$c_{O_2} = c^0_{O_2} \exp\left(-\frac{\Delta G_{diss}}{RT}\right) \quad (4)$$

Henry's law can be used to relate the solubility of O_2 in H^+ Nafion® membrane to the partial pressure of O_2 in the gas phase [46]:

$$c_{O_2} = \frac{p_{O_2}}{K_H} \quad (5)$$

where K_H is the Henry's constant. Eq. (5) means the solubility of oxygen in the membrane is proportional to the partial pressure of oxygen in the gas mixture. The saturated water vapor pressure is constant in the fuel cell and equals p_{sat} = 31.164 kPa at 70 °C. Since it is a relatively small cell, it is assumed that the partial pressure of O_2 is uniform everywhere, which is equal to

$$p_{O_2} = (P_t - p_{sat}) \times 0.21 \quad (6)$$

where 0.21 is the molar fraction of O_2 in air.

Values of D_{O_2} (T = 50 °C), K_H (T = 50 °C), E_{diff}, and ΔG_{diss} are listed in Table 1. Diffusion coefficient of O_2 at T = 70 °C can be calculated with Eq. (3) directly. Solubility of O_2 at T = 70 °C can be calculated with Eqs. (4)–(6). The fluxes of O_2 (N_{O_2}) through 25 and 5 μm hydrated Gore Select® membranes at T = 70 °C are shown in Table 2.

Table 1
Parameters for calculating molar flux of O_2 in hydrated H^+ membrane.

D_{O_2} ($\times 10^6$ cm^2 s^{-1})	2.05 (50 °C)[a]
K_H ($\times 10^{-7}$ kPa cm^3 mol^{-1})	2.68 (50 °C)[a]
E_{diff} (kJ mol^{-1})	24.9[b]
ΔG_{diss} (kJ mol^{-1})	−5.53[b]

[a] From Ref. [46].
[b] From Ref. [45].

Table 2
Molar flux of O_2 through the membrane under different cathode backpressures for 25 and 5 μm CCMs (T = 70 °C).

Cathode backpressures (kPa)	101.33		303.98	
Oxygen partial pressures (kPa)	14.734		57.290	
CCM thickness (μm)	25	5	25	5
Molar flux for O_2 ($\times 10^7$ mol cm^{-2} s^{-1})	0.0068	0.034	0.027	0.13

4. Modeling

The internal air bleed can oxidize the CO in the anode chemically. It was proposed by Giorgi et al. [47] that electrochemical oxidation of H_2 on Pt–Ru/C follows a Heyrovski–Volmer mechanism, which

can be written as

$$\mathrm{Pt} + \mathrm{H_2} \underset{b_{fh}k_{fh}}{\overset{k_{fh}}{\leftrightarrow}} \mathrm{Pt\text{–}H_2} \quad (7)$$

$$\mathrm{Pt\text{–}H_2} \overset{k_{eh}}{\leftrightarrow} \mathrm{Pt} + 2\mathrm{H^+} + 2e^- \quad (8)$$

Since Ru–OH is only involved in the oxidation of CO under relatively higher anode potential [21] and the anode overpotential obtained in this work is fairly small (<0.1 V), no contribution of oxidation of CO by Ru–OH will be included in the modeling equations. The presence of Ru in a Pt–Ru anode only changes the adsorption and desorption constants of CO on Pt:

$$\mathrm{Pt} + \mathrm{CO} \underset{b_{fc}k_{fc}}{\overset{k_{fc}}{\leftrightarrow}} \mathrm{Pt\text{–}CO} \quad (9)$$

Therefore, the CO poisoning and the effect of internal air bleed can be studied by modifying the equations of Springer et al. [48] and Nwoga and Van Zee [49–51] by including only a consumption term ($2\gamma N_{\mathrm{O_2}}$) in the balance for CO sites:

$$c_t \frac{d\theta_{\mathrm{H_2}}}{dt} = k_{fh} p_{\mathrm{H_2}} (1 - \theta_{\mathrm{CO}} - \theta_{\mathrm{H_2}}) - b_{fh} k_{fh} \theta_{\mathrm{H_2}} - \frac{i_h}{2F} \quad (10)$$

$$c_t \frac{d\theta_{\mathrm{CO}}}{dt} = k_{fc} p_{\mathrm{CO}} (1 - \theta_{\mathrm{CO}} - \theta_{\mathrm{H_2}}) - b_{fc} k_{fc} \theta_{\mathrm{CO}} - 2\gamma N_{\mathrm{O_2}} \quad (11)$$

where γ is the fraction of O_2 diffused to anode that oxidizes CO, $0 \le \gamma \le 1$, $N_{\mathrm{O_2}}$ is the molar flux of O_2, which is a constant calculated according to Eqs. (2)–(6), and c_t is the molar area density of catalyst sites. The partial pressures of CO and H_2 are as follows:

$$p_{\mathrm{H_2}} = p_{atm} - p_{sat} \quad (12)$$

$$p_{\mathrm{CO}} = (p_{atm} - p_{sat}) \times 50 \times 10^{-6} \quad (13)$$

Although there will be some trace amount of CO diffusing through the membrane to the cathode side [52], it does not seem to affect the cathode side too much since the cathode side is highly oxidative and the diffused CO to the cathode side will meet a huge air bleed during normal fuel cell operation. The rate expression for H_2 oxidation is assumed to obey the Butler–Volmer equation and if we only analyze the region prior to CO oxidation, H_2 oxidation is equal to the total current density of the fuel cell. That is,

$$\frac{i}{2F} = \frac{i_h}{2F} = k_{eh}\theta_{\mathrm{H_2}} \left(\exp\left[\frac{(1-\beta_{\mathrm{H_2}})nF\eta_a}{RT}\right] - \exp\left[-\frac{\beta_{\mathrm{H_2}}nF\eta_a}{RT}\right] \right) \quad (14)$$

where η_a is the overpotential calculated from the experiment as described in Refs. [38,53]. The flux ($N_{\mathrm{O_2}}$) is calculated by assuming the concentration of O_2 on the anode to be 0. This assumption of zero concentration is justified by considering that the O_2 adsorption isotherm favors O_2 in the gas phase and by considering that any adsorbed O_2 is reacted with either H_2 or CO. In addition, zero concentration implies that a site balance for O_2 similar to Eq. (10) is not necessary. Then without a surface concentration of O_2 (i.e., $\theta_o = 0$), the H_2 isotherm parameter (b_{fh}), the electrochemical rate constants (k_{eh} and $\beta_{\mathrm{H_2}}$), and the CO rate constant (k_{fc}) obtained by Nwoga and Van Zee [51,52] for these Pt–Ru electrodes can be used as shown in Table 3. Note that the CO isotherm equilibrium constant, b_{fc}, was shown to change with pressure and CO concentration [51]. A new value for k_{fh} was used which is very close to the values in Ref. [52].

Table 3
Model parameters for CO and H_2 on PRIMEA® 5561 MEAs (70 °C)[a].

$\beta_{\mathrm{H_2}}$	0.5
b_{fh}	5.74×10^5 Pa
k_{eh}	9.85×10^{-5} mol cm^{-2} s^{-1}
k_{fc}	5.13×10^{-10} mol Pa^{-1} cm^{-2} s^{-1}

[a] From Refs. [51,52].

One would expect that γ is dependent on the surface coverage of H_2 ($\theta_{\mathrm{H_2}}$) and CO (θ_{CO}) and the cathode pressure of O_2 under different operating conditions and CCM thicknesses. Since $\gamma = fun(\theta_{\mathrm{H_2}}, \theta_{\mathrm{CO}}, p_{\mathrm{O_2}}, t_m)$, we choose to fit this parameter according to a minimum in the sum of the squares of the difference in predicted and experimental values of η_a. Thus the exercise is to fit these anode overpotential data with the simultaneous numerical solution of the steady-state versions of Eqs. (10), (11) and (14) to obtain the best values of γ at each $p_{\mathrm{O_2}}$ and t_m. Note that we expect the value of γ to change because the residence time of O_2 could vary under different operating conditions. This expectation is analyzed further below.

The results of the minimization process for obtaining γ are shown in Table 4. Figs. 3 and 4 show the comparison of the simulation and experimental results for 5 and 25 μm CCMs under different cathode backpressures. The simulation results agree very well with the experimental data under anode potential where there is no electro-oxidation of CO by Ru–OH. As can be seen from Table 4, the net amount of diffused O_2 used for CO oxidation ($\gamma N_{\mathrm{O_2}}$) increases with the increase of cathode backpressure for both CCMs for 50 ppm CO in H_2. Hence, the surface coverage of CO decreases with the increase of the cathode backpressure as would be expected. A larger $\gamma N_{\mathrm{O_2}}$ yields a smaller value of the anode overpotential. The values of the sum of the square of the errors (i.e., the objective function) are also shown in Table 4.

Further analysis of these data is possible with this model. Since γ is very small for all the cases, the reaction rate constant of the overall non-electrochemical reaction is very small compared with the adsorption rate constant of CO. That is,

$$\mathrm{O_2} + 2\mathrm{CO} \rightarrow 2\mathrm{CO_2} \quad (15)$$

Reaction (15) can be written as a sum of two surface reactions:

$$\mathrm{Pt} + 1/2\mathrm{O_2} \rightarrow \mathrm{Pt\text{–}O} \qquad k_1 \quad (16)$$

$$\mathrm{Pt\text{–}CO} + \mathrm{Pt\text{–}O} \rightarrow 2\mathrm{Pt} + \mathrm{CO_2} \qquad k_{\mathrm{CO}} \quad (17)$$

Table 4
Surface coverages of CO, H_2 and internal air bleed coefficients for 50-ppm CO/H_2 under different cathode backpressures (T_{cell} = 70 °C).

Partial pressure of CO (Pa)	3.5	3.5	3.5	3.5
CCM thickness (μm)	5	5	25	25
Cathode backpressure (kPa)	101	303	101	303
θ_{CO}	0.564 ± 0.007	0.025 ± 0.007	0.650 ± 0.006	0.451 ± 0.006
$\theta_{\mathrm{H_2}}$	0.076 ± 0.008	0.177 ± 0.008	0.060 ± 0.007	0.098 ± 0.007
γ	0.0359	0.0439	0.0354	0.0333
$\gamma N_{\mathrm{O_2}}$ ($\times 10^{-10}$ mol cm^{-2} s^{-1})	0.55	2.67	0.24	0.90
k_{fh} ($\times 10^{-9}$ mol cm^{-2} s^{-1} Pa^{-1})	0.86	0.86	0.86	0.86
b_{fc} (Pa)	0.477	0.477	0.477	0.477
$\sum \eta_{a,ex}^2$	0.068	0.0012	0.042	0.0038
$\Sigma(\eta_{a,ex} - \eta_{a,th})^2$	1.8×10^{-5}	1.6×10^{-6}	4.0×10^{-4}	2.1×10^{-5}
Number of data points	18	18	16	16

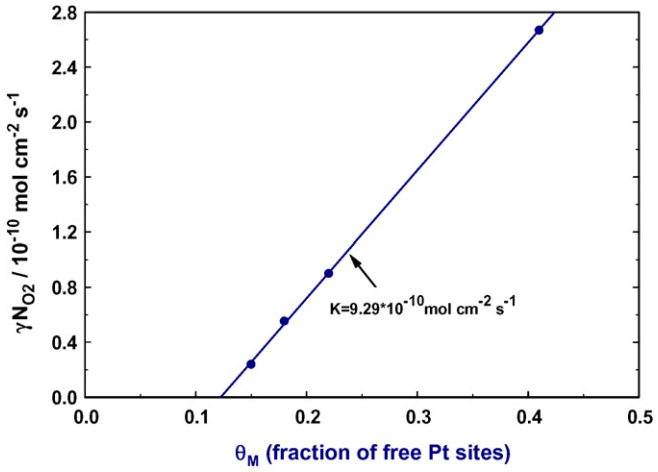

Fig. 5. Regression line using all the (θ_M, $\gamma^* N_{O_2}$) data points for CO oxidation by internal air bleed.

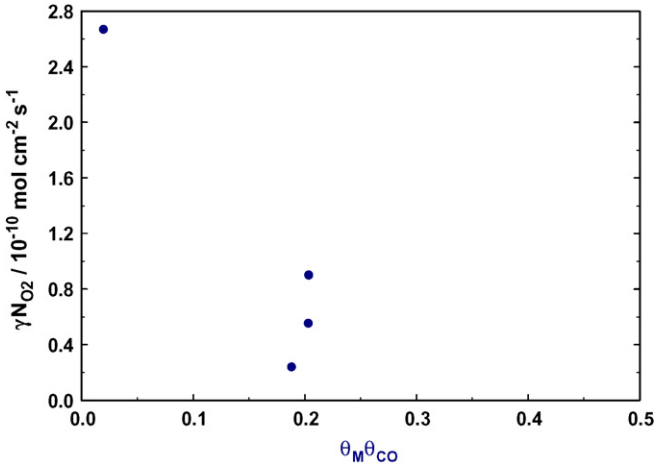

Fig. 6. Regression line using all the ($\theta_M\theta_{CO}$, $\gamma^* N_{O_2}$) data points for CO oxidation by internal air bleed.

If reaction (16) determines the rate of oxidation of CO by O_2, then the rate expression can be written (assuming the coverage of Pt as Pt–O (i.e., θ_o) is small).

$$\theta_M \approx 1 - \theta_{CO} - \theta_{H_2} \tag{18}$$

$$r = k_1 p_{O_2}^{1/2} \theta_M = k_1 p_{O_2}^{1/2} (1 - \theta_{CO} - \theta_{H_2}) \tag{19}$$

Similarly, if reaction (17) controls the oxidation of CO, the rate can be written:

$$r = k_{CO} \theta_{CO} \theta_o \tag{20}$$

$$K_{eq} = \frac{\theta_o}{\theta_M \; p_{O_2}^{1/2}} \tag{21}$$

where K_{eq} is the equilibrium constant of reaction (16).

Eq. (20) can be rewritten as follows:

$$r = k_{CO} K_{eq} p_{O_2}^{1/2} (1 - \theta_{CO} - \theta_{H_2}) \theta_{CO} = k_{CO} K_{eq} p_{O_2}^{1/2} \theta_M \theta_{CO} \tag{22}$$

Then a preliminary indication of the rate-controlling step can be obtained by plotting $r = \gamma N_{O_2}$ versus θ_M or $\theta_M\theta_{CO}$ depending on the expression for r. The slope, K, will be a lumped rate constant equal to either $K = k_1 p_{O_2}^{1/2}$ or $K = k_{CO} K_{eq} p_{O_2}^{1/2}$. Figs. 5 and 6 show this analysis. However, the ability to correlate linearly the rate with θ_M in Fig. 5 and the inability for the rate to correlate with $\theta_M\theta_{CO}$ in Fig. 6 indicates that reaction (16) is the correct rate-limiting step for internal air bleed with these thin CCMs. The regression line for Fig. 5 is

$$r = K(\theta_M - \theta_{M0}) = 9.29 \times 10^{-10} \times (\theta_M - 0.12) \tag{23}$$

When $\theta_{M0} \leq 0.12$, r is negative, which means that the effect of internal air bleed can be ignored for high concentration of CO in H_2. However, Eq. (23) can be useful for the analysis of lower levels of CO contaminants in H_2 or H_2-rich reformate gas.

5. Conclusions

An internal air bleed proves effective for the mitigation of CO poisoning for a Pt/Ru anode under high cathode backpressure for 5 and 25 μm CCMs operating with 50 ppm CO/H_2. The anode overpotential decreases with the increase of cathode backpressure if the cathode backpressure is increased or a thinner CCM is used. That can be explained by the oxidation of CO by more O_2 diffusing from cathode to anode for a higher cathode backpressure or a thinner membrane.

A model accounting for the internal air bleed is proposed to explain the observed effects of cathode backpressure and membrane thickness on anode polarization. The modeling results agree very well with the experimental data using the model proposed. The small values of γ are probably a result of low O_2 adsorption on the catalyst surface rather than a slow reaction of Pt–CO and Pt–O surface species. The modeling results further show that a portion of the internal air bleed is used for the oxidation of CO even at ambient condition. Therefore, the internal air bleed needs to be included in the modeling of anode polarization or overall fuel cell performance when CO/H_2 system is used as the anode fuel gas, especially when the CO concentration is very low and the membrane is ultra-thin. An empirical relationship between γN_{O_2} and fraction of free Pt sites is provided for facilitating the inclusion of the effect of the internal air bleed in numerical modeling for a PEMFC with relatively thin membranes.

Acknowledgements

The authors gratefully acknowledge that W.L. Gore & Associates, Inc. provided the CCMs.

And Prof. John W. Van Zee and Tochi Nwoga of the University of South Carolina helped with the analysis of the parameters for the modeling equations.

References

[1] R.J. Bellows, E.P. Marucchi-Soos, D.T. Buckley, Ind. Eng. Chem. Res. 35 (1996) 1235.
[2] S. Gottesfeld, J. Pafford, J. Electrochem. Soc. 135 (1998) 2651–2652.
[3] T. Engel, G. Ertle, in: D. King, D. Woodruff (Eds.), The Chemical Physics of Solid Substances and Heterogeneous Catalysis, vol. 4, Elsevier, Amsterdam, 1982, pp. 73–93.
[4] M. Schimidt, H.-F. Oetjen, J. Divisek, J. Electrochem. Soc. 144 (9) (1997) L237–L238.
[5] R.J. Bellows, E. Marucchi-soos, R.P. Reynolds, Electrochem. Solid-State Lett. 1 (2) (1998) 69–70.
[6] S.J. Lee, S. Mukerjee, E.A. Ticianelli, J. McBreen, Electrochim. Acta 44 (1999) 3283–3293.
[7] G.A. Camara, E.A. Ticianelli, S. Mukerjee, S.J. Lee, J. McBreen, J. Electrochem. Soc. 149 (2002) A748–A753.
[8] C. He, H.R. Kunz, J.M. Fenton, J. Electrochem. Soc. 150 (2003) A1017–A1024.
[9] J.X. Wang, S.R. Brankovic, Y. Zhu, J.C. Hanson, R.R. Adžic, J. Electrochem. Soc. 150 (2003) A1108–A1117.
[10] D.C. Papageorgopoulos, M.P. de Heer, M. Keijzer, J.A.Z. Pieterse, F.A. de Bruijn, J. Electrochem. Soc. 151 (2004) A763–A768.
[11] R.C. Urian, A.F. Gullá, S. Mukerjee, J. Electroanal. Chem. 307 (2003) 554–555.
[12] Z. Qi, A. Kaufman, J. Power Sources 113 (2003) 115–123.
[13] Y. Kawasoe, S. Tanaka, T. Kuroki, H. Kusaba, K. Ito, Y. Teraoka, K. Sasaki, J. Electrochem. Soc. 154 (2007) B969–B975.
[14] B.N. Grgur, N.M. Markovic, P.N. Ross, J. Electrochem. Soc. 146 (1999) 1613–1619.

[15] T. Ioroi, K. Yasuda, Z. Siroma, N. Fujiwara, Y. Miyazaki, J. Electrochem. Soc. 150 (2003) A1225–A1230.
[16] S. Mukerjee, R.C. Urian, S.J. Lee, E.A. Ticianelli, J. McBreen, J. Electrochem. Soc. 151 (2004) A1094–A1103.
[17] E.I. Saniago, M.S. Batista, E.M. Assaf, E.A. Ticianelli, J. Electrochem. Soc. 151 (2004) A944–A949.
[18] D.A. Stevens, J.M. Rouleau, R.E. Mar, R.T. Atanasoski, A.K. Schmoeckel, M.K. Debe, J.R. Dahn, J. Electrochem. Soc. 154 (2007) B1211–B1219.
[19] M. Watanabe, S. Motoo, J. Electroanal. Chem. 60 (1975) 267.
[20] M. Watanabe, S. Motoo, J. Electroanal. Chem. 60 (1975) 275.
[21] H.A. Gasteiger, N. Markovic, P.N. Ross Jr., E.J. Cairns, J. Phys. Chem. 98 (1994) 617.
[22] F. Buatier de Mongeot, M. Scherer, B. Gleich, E. Kopatzki, R.J. Behm, Surf. Sci. 411 (1998) 249–262.
[23] M. Murthy, M. Esayian, A. Hobson, S. MacKenzie, W.-K. Lee, J.W. Van Zee, J. Electrochem. Soc. 148 (2001) A1141–A1147.
[24] B. Rohland, V. Plzak, J. Power Sources 84 (1999) 183–186.
[25] W. Shi, M. Hou, Z. Shao, J. Hu, Z. Hou, P. Ming, B. Yi, J. Power Sources 174 (2007) 164–169.
[26] A.T. Haug, R.E. White, J.W. Weidner, W. Huang, J. Electrochem. Soc. 149 (2002) A862–A867.
[27] A.T. Haug, R.E. White, J.W. Weidner, W. Huang, S. Shi, N. Rana, S. Grunow, T.C. Stoner, A.E. Kaloyeros, J. Electrochem. Soc. 149 (2002) A868–A872.
[28] F.A. Uribe, J.A. Valerio, F.H. Garzon, T.A. Zawodzinski, Electrochem. Solid-State Lett. 7 (2004) A376–A379.
[29] P.A. Adcock, S.V. Pacheco, K.M. Norman, F.A. Uribe, J. Electrochem. Soc. 152 (2005) A459–A466.
[30] Z. Ogumi, Z. Takehara, S. Yoshizawa, J. Electrochem. Soc. 131 (4) (1984) 769–773.
[31] Z. Ogumi, T. Kuroe, Z. Takehara, J. Electrochem. Soc. 132 (11) (1985) 2601–2605.
[32] S. Gottesfeld, I.D. Raistrick, S. Srinivasan, J. Electrochem. Soc. 134 (6) (1987) 2601–2605.
[33] T. Lehtinen, G. Sundholm, S. Holmberg, F. Sundholm, P. Björnbom, M. Bursell, Electrochim. Acta 43 (12–13) (1998) 1881–1890.
[34] A.T. Haug, R.E. White, J. Electrochem. Soc. 147 (3) (2000) 980–983.
[35] A. Parthasarathy, C.R. Martin, S. Srinivasan, J. Electrochem. Soc. 138 (4) (1991) 916–921.
[36] A. Parthasarathy, S. Srinivasan, A.J. Appleby, J. Electrochem. Soc. 139 (1992) 2530–2537.
[37] P. Gode, G. Lindbergh, G. Sundholm, J. Electroanal. Chem. 518 (2002) 115–122.
[38] J. Zhang, T. Thampan, R. Datta, J. Electrochem. Soc. 149 (6) (2002) A765–A772.
[39] W.-K. Lee, J.W. Van Zee, S. Shimpalee, S. Dutta, Proceedings of the ASME IMECE, vol. 5, 1999, pp. 454–460.
[40] B. Du, R. Pollard, J.F. Elter, ECS Trans. 3 (1) (2004) 705–713.
[41] B. Bahar, A.R. Hobson, J.A. Kolde, Internal composite membrane, United States, patent no. RE37701 (2002).
[42] W. Liu, K. Ruth, G. Rusch, J. New Mater. Electrochem. Syst. 4 (2001) 227–232.
[43] M.A.V. Devanathan, Z. Stachurski, Proc. R. Soc., Edinburgh, Sect. A 270 (1962) 90.
[44] M.C. Kimble, R.E. White, Y. Tsou, R.N. Beaver, J. Electrochem. Soc. 137 (1990) 2510–2514.
[45] A. Parthasarathy, S. Srinivasan, A.J. Appleby, C.R. Martin, J. Electrochem. Soc. 139 (9) (1992) 2530–2537.
[46] A. Parthasarathy, S. Srinivasan, A.J. Appleby, J. Electrochem. Soc. 139 (10) (1992) 2856–2862.
[47] L. Giorgi, A. Pozio, C. Bracchini, R. Giorgi, S. Turtu, J. Appl. Electrochem. 31 (2001) 325–334.
[48] T.E. Springer, T. Rockward, T.A. Zawodzinksi, S. Gottesfeld, J. Electrochem. Soc. 148 (2001) A11–A23.
[49] T.T. Nwoga, J.W. Van Zee, paper#853, 202nd ECS Meeting, Salt Lake City, October 2002.
[50] T.T. Nwoga, Ph.D. dissertation, Dept. of Chemical Engineering, University of South Carolina, Columbia, SC, 2007.
[51] T.T. Nwoga, J.W. Van Zee, Electrochem. Solid-State Lett. 11 (7) (2008) B122–B126.
[52] Z. Qi, C. He, A. Kaufman, Electrochem. Solid-State Lett. 4 (12) (2001) A204–A205.
[53] W. Wang, Ph.D. dissertation, Dept. of Chemical Engineering, University of South Carolina, Columbia, SC, 2006.